Instability at the Winter Stratopause: A Mechanism for the 4-Day Wave

G. L. MANNEY

Jet Propulsion Laboratory/California Institute of Technology, Pasadena, California

W. J. RANDEL

National Center for Atmospheric Research, Boulder, Colorado*

(Manuscript received 30 December 1992, in final form 12 May 1993)

ABSTRACT

Studies using climatological fields in a three-dimensional stability model show unstable modes near the polar winter stratopause with periods near 4 days. The calculated modes exhibit equatorward momentum and heat fluxes near the stratopause, similar to characteristics of observed 4-day wave events, demonstrating that both baroclinic and barotropic processes are important for this instability. The baroclinic and barotropic components are considered separately by selectively removing either horizontal or vertical shear from the background flow. Although both situations reveal instability, growth rates are very slow; realistic growth rates occur only for climatological flows including both horizontal and vertical shears. Similar unstable, fast-moving waves are found near the polar stratopause for several winter months in both hemispheres.

1. Introduction

A number of observational and theoretical studies have focused on the 4-day eastward propagating wave in the polar winter stratosphere, first identified by Venne and Stanford (1979). The observed characteristics have been summarized by Manney (1991) and Randel and Lait (1991). Briefly,

- The 4-day wave is a ubiquitous feature in the polar winter upper stratosphere (Manney 1991), and has been observed in both hemispheres (Venne and Stanford 1982). It is characterized by waves of zonal wavenumber 1 through at least 4, moving with approximately the same phase speed (Prata 1984; Lait and Stanford 1988) such that the wave 1 period is near 4 days.
- The horizontal phase structure of the 4-day wave is variable, with observations showing time periods with both poleward and equatorward momentum flux (Venne and Stanford 1982; Prata 1984; Manney 1991).
- In many cases, the 4-day wave shows small vertical phase tilts (Venne and Stanford 1982; Prata 1984) suggesting that the dynamics are fundamentally barotropic in character. However, Randel and Lait (1991) showed one episode where strong equatorward heat flux was associated with amplification of the 4-day wave, and thus the wave had a significant baroclinic component.

Hartmann (1983) and Manney et al. (1988) showed that episodes of 4-day wave growth associated with poleward momentum fluxes are consistent with barotropic instability of the stratospheric polar night jet. Manney (1991) confirmed this by doing stability calculations for basic-state winds from the times of specific cases where the observed 4-day wave was growing and was associated with poleward momentum flux.

Other episodes of 4-day wave growth are associated with equatorward momentum flux (Manney 1991; Randel and Lait 1991). These episodes tend to have peak geopotential amplitudes at the highest levels available in data (1 mb), and show evidence of amplifying earlier at higher altitudes; episodes with poleward momentum fluxes tend to peak at slightly lower altitudes (5 to 10 mb) and show no evidence of early amplification at higher levels. The equatorward momentum flux events appear to be consistent with instability of the "double jet" structure observed in the upper stratosphere and mesosphere (Manney 1991; Randel and Lait 1991). Randel and Lait (1991) showed that one episode in August 1980 with equatorward momentum fluxes was also associated with strong equatorward heat flux in the polar upper stratosphere. This equatorward heat transport is downgradient to the background of the warm polar stratopause. Furthermore, analysis of the stability of climatological wind fields showed that a significant portion of the in-

* The National Center for Atmospheric Research is sponsered by the National Science Foundation.

Corresponding author address: Gloria L. Manney, JPL, Mail Stop 183-701, California Institute of Technology, 4800 Oak Grove Drive, Pasadena, CA 91109.

stability of the winter stratopause region is due to the strong horizontal temperature gradients (as shown below). Thus, it is suggested (Randel and Lait 1991) that the generation of the 4-day wave could be due in part to baroclinic instability at the stratopause.

In the following, a stability analysis is done for the polar upper stratosphere and mesosphere in winter using a model that allows full vertical and meridional variations in the basic state, using basic states taken from climatological data. We show that characteristics of calculated unstable modes are in good agreement with observations of the 4-day wave. The baroclinic and barotropic components of this instability are considered separately by smoothing the background flow in either latitude or height. Results show that both horizontal and vertical shears are necessary for realistic growth rates to occur in climatological flow (although this may not be the case for synoptic or daily conditions). Similar unstable modes are found for several winter months in both hemispheres, with periods of 3 to 5 days; these periods are mainly determined by the advective time scale of the zonal wind near the polar stratopause.

2. The model and basic states

The stability model was developed by Elson (1989, 1990) and is also described by Manney (1991). This three-dimensional model includes realistic meridional and vertical variations in a zonally symmetric basic flow. The linearized quasigeostrophic potential vorticity equation with a constant Newtonian cooling ($1/20$ d^{-1}) is solved on a sphere using a log-pressure vertical coordinate. The solution yields a complex frequency (giving period and growth rate) and perturbation streamfunction for the most unstable mode at a given zonal wavenumber. In the calculations presented here, the perturbation streamfunction is set to zero at both vertical boundaries (at 30 mb and 0.01 mb) and lateral boundaries (at $-80°$ and $-20°$ for Southern Hemisphere runs and 20° and 80° for Northern Hemisphere runs).

Basic states are derived from data given in the climatology of Fleming et al. (1988), which gives monthly climatological zonal-mean fields of geopotential height, temperature, and zonal wind from 0 to 120 km. To obtain a basic state for the model, geopotential heights from Fleming et al. (1988) are interpolated onto the model grid (45 points in the horizontal by 20 in the vertical), and zonal-mean wind and temperature fields are calculated from these via geostrophic and hydrostatic approximations. Cases have also been run for winds calculated using the gradient wind approximation; results are very similar, with slightly slower growth rates. Potential vorticity (PV) gradients for these basic states are close to those shown by Fleming et al. (1988, calculated using gradient winds), but with slightly stronger negative values.

We present detailed results for stability calculations in the Southern Hemisphere using August climatological fields, since the August wind fields suggest the strongest instability characteristics. We also include calculations for fields that have been smoothed to make either the horizontal or vertical term in the PV gradient the dominant contributor to the change in sign, in an attempt to isolate individual baroclinic or barotropic components. We briefly present results for other winter months in both Northern and Southern hemispheres.

3. Model results

Figure 1 shows the basic-state zonal-mean wind field, $\bar{u}$, for August, along with the potential vorticity (PV) gradient, $\bar{q}_y$, defined by

$$\bar{q}_y = \frac{2\Omega}{a}\cos\phi - \frac{1}{a^2}\frac{\partial}{\partial\phi}\left[\frac{1}{\cos\phi}\frac{\partial}{\partial\phi}(\bar{u}\cos\phi)\right] - (2\Omega\sin\phi)^2\rho_0^{-1}\frac{\partial}{\partial z}\left(\rho_0\frac{1}{N^2}\frac{\partial\bar{u}}{\partial z}\right)$$
$$= \quad \beta \quad + \quad Q_H \quad + \quad Q_V.$$

We have separated the components due to horizontal (Q_H) and vertical (Q_V) shears of the zonal wind. Intuitively, unstable modes resulting from horizontal shears will be predominantly barotropic and those resulting from vertical shears predominantly baroclinic (this is confirmed below). For the August climatological fields in Fig. 1, the maximum negative value of the vertical term is slightly larger than that of the horizontal term, and the location of these regions is such that they combine with β to produce a field with a larger and deeper region of negative PV gradients, centered near 55°S and 60 km.

The results of the stability calculation for this basic state are shown in Fig. 2 for zonal wavenumber 1. Temperature perturbations are shown since they are directly comparable to observations in satellite data. The period and e-folding times for this mode are 4.18 d, and 4.38 d, respectively. The perturbation temperature field shown in Fig. 2a has a double-lobed structure, with amplitude maxima in the upper stratosphere and mesosphere and a rapid phase change between. Momentum fluxes, heat fluxes, and Eliassen–Palm (EP) fluxes and EP flux divergence are shown in Figs. 2b–d, respectively. The EP fluxes and EP flux diver-

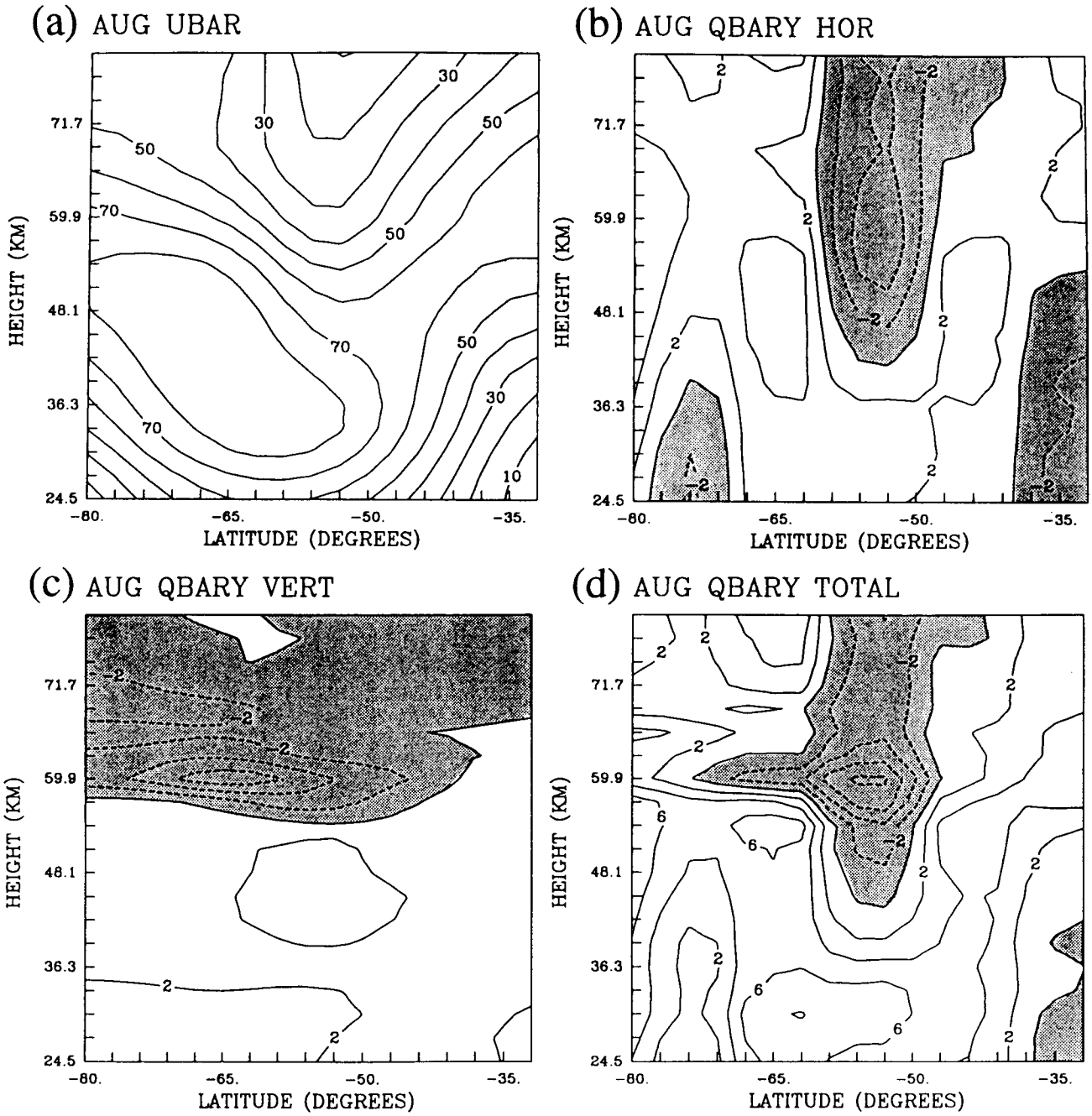

FIG. 1. Climatological zonal-mean wind field and potential vorticity gradients for August used as a basic state in the stability model: (a) zonal-mean zonal wind in meters per second, (b) horizontal term, Q_H, in the potential vorticity gradient, (c) vertical term, Q_V, in the potential vorticity gradient, and (d) total PV gradient, $\bar{q}_y$. See text for exact definition of terms in PV gradient.

gence are related to energy conversion as described by Plumb (1983). Momentum and heat fluxes are scaled so that they have the same relative magnitudes they would have if both were in MKS units; these scaled values are used to calculate the EP fluxes. The rapid change in sign of the heat fluxes across the stratopause reflects the rapid phase variation that occurs between the two amplitude maxima. In the region of the upper-stratospheric maximum, both momentum and heat fluxes are equatorward, and, as can be seen in Fig. 2d, their contributions are approximately equal. Strong positive EP flux divergence (identifying the source of wave activity) is located near 60°S and 60 km, spatially coincident with the maximum negative PV gradient

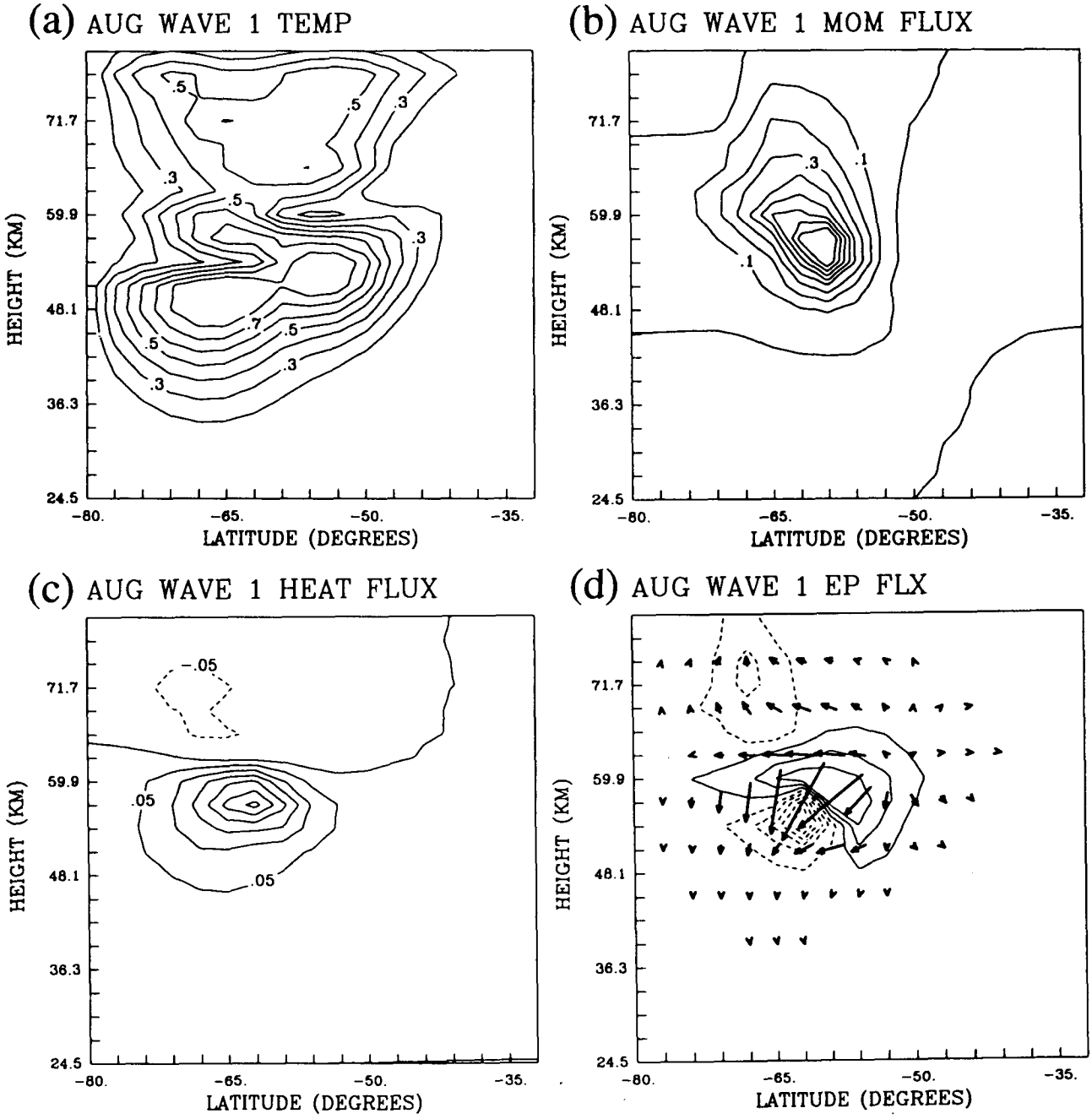

FIG. 2. Results from stability model for August basic state. (a) Perturbation temperature field for most unstable wave 1 mode, with maximum value normalized to 1, (b) perturbation momentum fluxes, (c) perturbation heat fluxes, scaled so that the relative amplitudes are as they would be if using MKS units; and (d) Eliassen–Palm (EP) flux and EP flux divergence for wave 1 unstable mode. Positive values (solid lines) show equatorward heat and momentum fluxes in (b) and (c).

seen in Fig. 1d. This spatial coincidence clearly identifies the source region for this instability (see Hartmann 1983; Randel and Lait 1991).

For comparison, Fig. 3 shows the zonal-mean wind and 4-day wave EP fluxes calculated by Randel and Lait (1991) for the episode in late August 1980 where strong equatorward heat fluxes were observed, plotted on the same domain as Fig. 2. The observed and calculated EP flux patterns are similar in that the vectors point downward and poleward (equatorward heat and momentum fluxes), with a north–south dipole pattern of flux divergence (the calculated pattern in Fig. 2d looks similar if only the lower half is considered). The calculated mode appears to be centered at slightly

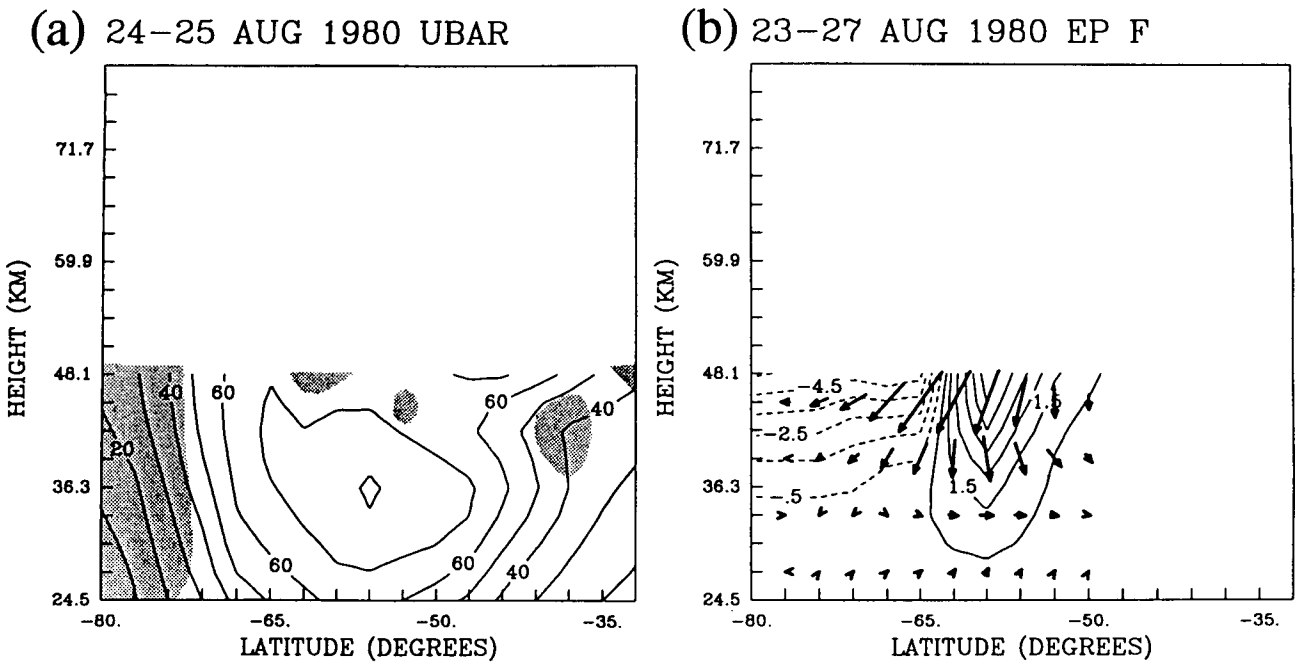

FIG. 3. (a) Zonal-mean wind (shading indicates regions where potential vorticity gradient is negative) and (b) EP fluxes and divergence from observations of the 4-day wave during late August 1980 (note that data are only available below the 1-mb level, or about 49 km; adapted from Randel and Lait 1991).

higher altitude, although the lack of observed data above 1 mb makes this uncertain. Overall, the qualitative features are consistent between calculated and observed modes.

Figure 4 shows temperatures and EP fluxes for the unstable modes at zonal wavenumbers 2 and 3 obtained from the stability model for the August basic flow. The rotation period (defined as the time for the wave to make a complete circuit of the globe, i.e., period times zonal wavenumber) for wave 2 is 4.13 d and the *e*-folding time is 4.22 d. For wave 3, the rotation period and *e*-folding times are 4.33 d and 17.9 d, respectively. The spatial structure of perturbation temperatures for waves 2 and 3 are similar to that of wave 1, with each higher wavenumber being somewhat more localized in horizontal and vertical extent, and having maximum amplitudes at successively more equatorward latitudes. Wave 2 EP fluxes are similar to those for wave 1, while those for wave 3 have smaller vertical components that point upward in the upper stratosphere. These features are all consistent with features of the individual wavenumber components shown by Randel and Lait (1991) for the August 1980 case (their Fig. 9). While the growth rate in a linear model does not necessarily determine which wave will achieve the largest amplitude, it is suggestive that the growth rate of wave 3 is much slower, consistent with observations that show wave 3 with much smaller amplitude than waves 1 and 2.

To examine the relative effect of vertical and horizontal shears in the basic flow, modified basic states have been used in stability calculations. These are as follows:

1) The August basic state is smoothed in the horizontal so that the minimum value of the horizontal term in the PV gradient (Q_H) is approximately zero, but the vertical term (Q_V) is still similar to that shown in Fig. 1.

2) The August basic state is smoothed in the vertical so that the minimum value of the vertical term in the PV (Q_V) gradient is approximately zero, with the horizontal term (Q_H) similar to that shown in Fig. 1.

While the smoothing necessarily alters the entire basic states to some extent, these fields still represent typical horizontal or vertical potential vorticity gradients for this time period. Figure 5 shows perturbation temperatures and EP fluxes for the unstable wave 1 mode for these cases. For case 1, the period and *e*-folding time are 2.53 d and 55 d. Case 1, where only the vertical term contributes to the instability, is much more localized than the full case shown in Fig. 2, with most of the amplitude being at and slightly below the stratopause, and closer to the pole than for the climatological flow. The EP fluxes are mainly downward (equatorward heat flux), confirming the intuitive notion that baroclinically unstable flow is associated with baroclinic wave structure. The unstable wave 2 mode in this case has a rotation period of 2.61 d, and an *e*-folding time of 32 d, with spatial structure nearly identical to that for wave 1. The periods of these modes

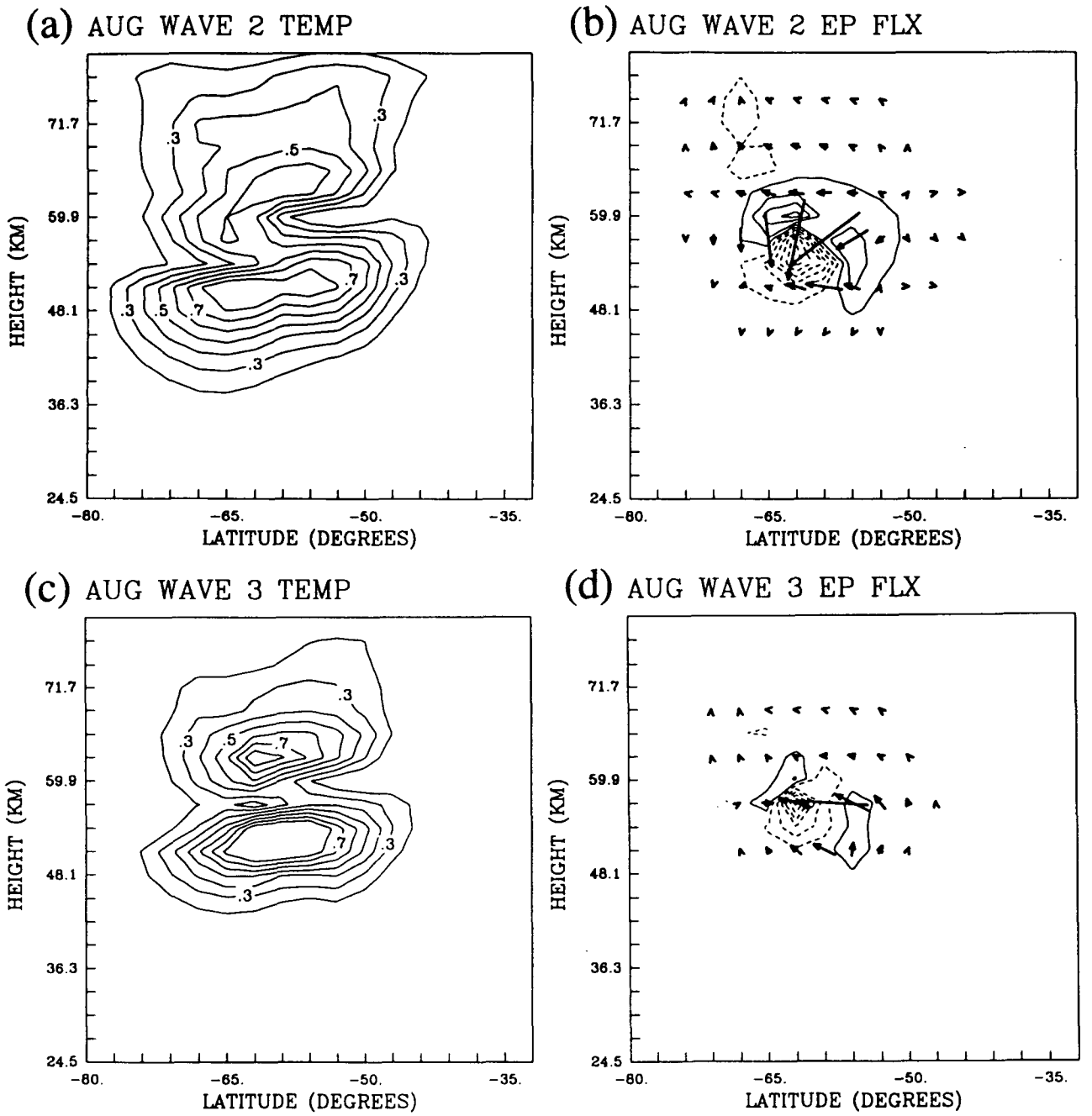

FIG. 4. Perturbation temperature fields and EP fluxes and divergences for most unstable wave 2 (a) and (b) and wave 3 (c) and (d) modes from model for basic state shown in Fig. 1. Scaling is as in Fig. 2.

are shorter than for those in the complete case; in fact, the largest amplitudes are confined to regions with stronger basic-state winds.

Case 2, where only the horizontal term contributes to the instability, shows a mode confined to the mesosphere, with strong equatorward momentum flux and weak poleward heat flux. Again, the intuitive notion that barotropic instability leads to barotropic wave modes is confirmed, and also the seat of the unstable region (near 55°S—see Fig. 1b) is identified by the positive EP flux divergence. The wave 1 periods and *e*-folding times for case 2 are 8.88 d and 17.7 d, respectively. The longer period in this case is presumably due to the fact that the unstable mode grows in a region where background winds are much weaker.

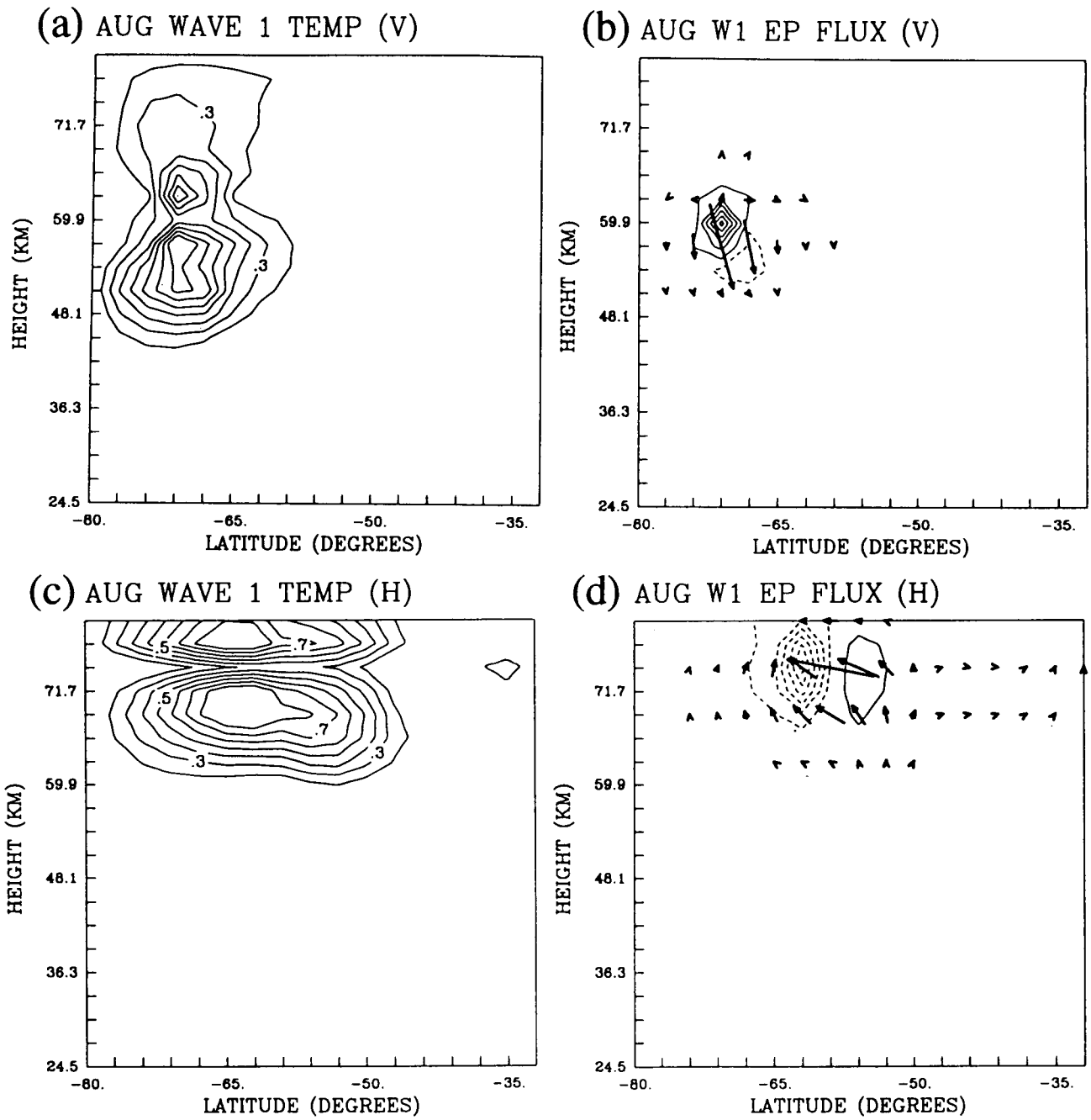

FIG. 5. Perturbation temperature fields and EP fluxes and divergences for most unstable wave 1 for cases where only vertical component (a) and (b) and horizontal component (c) and (d) contribute to the instability. See text for complete explanation of basic states used. Scaling is as in Fig. 2.

Growth rates for both case 1 and case 2 are greatly reduced over those for waves growing on the climatological basic state, and in fact are sufficiently small that more realistic dissipation and day to day variations in the flow would likely preclude any growth to finite amplitude. This is in contrast to the modes for the combined basic state, where *e*-folding times of less than one week are typical. This comparison indicates that both horizontal and vertical shears are necessary for a mode that is significantly unstable to grow on this climatological background state.

The instability model has also been run for wave 1 modes for basic states from June, July, and September in the Southern Hemisphere, and December, January,

February, and March in the Northern Hemisphere. Table 1 summarizes the results of the runs for each month, and gives the approximate wind speed in the region where the unstable mode has maximum amplitude, and the minimum (i.e., maximum negative) value of the horizontal (Q_H) and vertical (Q_V) terms of the PV gradient and of the total PV gradient, $\bar{q}_y$. In each month except March, there is an unstable wave 1 mode with a temperature structure similar to that observed for August in the Southern Hemisphere. Figure 6 shows the January Northern Hemisphere basic flow and potential vorticity gradients, and Fig. 7 shows the resulting unstable wave 1 mode. Although minimum values for the horizontal and vertical terms of the PV gradient are similar, the minimum for the horizontal term is near the top of the model, so the contribution from the vertical term is much larger in the region where the unstable mode forms. The EP fluxes show very strong downward components, indicating that the baroclinicity is particularly important in contributing to the instability in this case.

The periods of the unstable modes in Table 1 show a general inverse relationship with the background wind speed near the region of maximum wave amplitude, with periods being similar to the advective time scales (given by $2\pi a \cos\phi/\bar{u}$). This correspondence is not exact since the periods depend on the wind speeds throughout the region where the wave is growing. The e-folding times also show some correspondence with the magnitude of negative PV gradient, to the extent that the most unstable modes occur for cases with the strongest negative PV gradients (June, August, and December). This is only a very vague correspondence, since the degree of instability also depends on the steepness and location of the region of negative PV gradient.

4. Discussion and conclusions

A stability model has been run using zonal-mean basic states with realistic horizontal and vertical structure for the polar winter upper stratosphere and lower mesosphere. Basic states were derived from climatological monthly and zonal-mean geopotential heights. It is found that these climatological fields are unstable to small amplitude waves near the stratopause, in particular, eastward-moving planetary-scale waves with similar phase speeds, such that the wave 1 period is near 4 days. Calculated modes with similar spatial structures are found for climatological states from June, July, August, and September in the Southern Hemisphere, and December, January, and February in the Northern Hemisphere. The spatial structure of the perturbation temperature field has two lobes, one in the upper stratosphere and one in the lower mesosphere, with rapid phase variation in between. Temperature amplitudes are usually somewhat larger in the lower (stratospheric) lobe. These unstable modes are characterized by equatorward momentum fluxes and equatorward heat fluxes in the stratosphere; these in turn are related to the structure of the basic flow. The basic-state temperature gradients here are the opposite of those usually considered in stability calculations (i.e., Simmons 1974), in that the pole is warmer than lower latitudes. Simmons (1974), in fact, found poleward heat flux in the stratosphere and equatorward heat flux in the mesosphere, opposite to the results shown here. The double-lobed structure is likely related to the change in static stability across the stratopause.

The relative importance of heat and momentum fluxes depends on the degree to which horizontal and vertical terms of the basic-state PV gradient are important in producing a region of net negative PV gradient. The wave periods show some correspondence to the wind speeds in the region of maximum wave amplitude, consistent with zonal advection playing a dominant role in determining the local wave period. The nondispersive character of these waves is in part related to the existence of a critical latitude near the latitude where the potential vorticity gradient changes sign, as discussed by Manney et al. (1988).

TABLE 1. Characteristics of climatological basic states and the resulting unstable zonal wavenumber 1 modes: $\bar{U}$ is the approximate wind speed in the region of maximum wave amplitude; min (Q_H), min (Q_v), and min ($\bar{q}_y$) are the largest negative values of horizontal, vertical, and total potential vorticity gradients (see text for exact definitions), in units of 10^{-11} m^{-1} s^{-1}; τ_r is the period, and τ_i the e-folding time. Some values are not shown for March, where basic state is only marginally unstable.

Case	$\bar{U}$ (m s^{-1})	min (Q_H)	min (Q_v)	min ($\bar{q}_y$)	τ_r (d)	τ_i (d)
			Southern Hemisphere			
Jun	75	−10	−3.0	−8.5	3.41	7.61
Jul	75	−6.6	−4.1	−7.5	3.40	9.57
Aug	55	−6.0	−7.5	−8.4	4.18	4.38
Sep	25	−4.0	−7.7	−7.6	6.61	16.7
			Northern Hemisphere			
Dec	60	−9.9	−3.5	−9.8	3.16	7.47
Jan	35	−5.5	−4.2	−5.3	4.88	19.2
Feb	30	−6.6	−4.6	−6.1	5.31	15.1
Mar		−4.0	−2.9	−3.2	12.2	>100

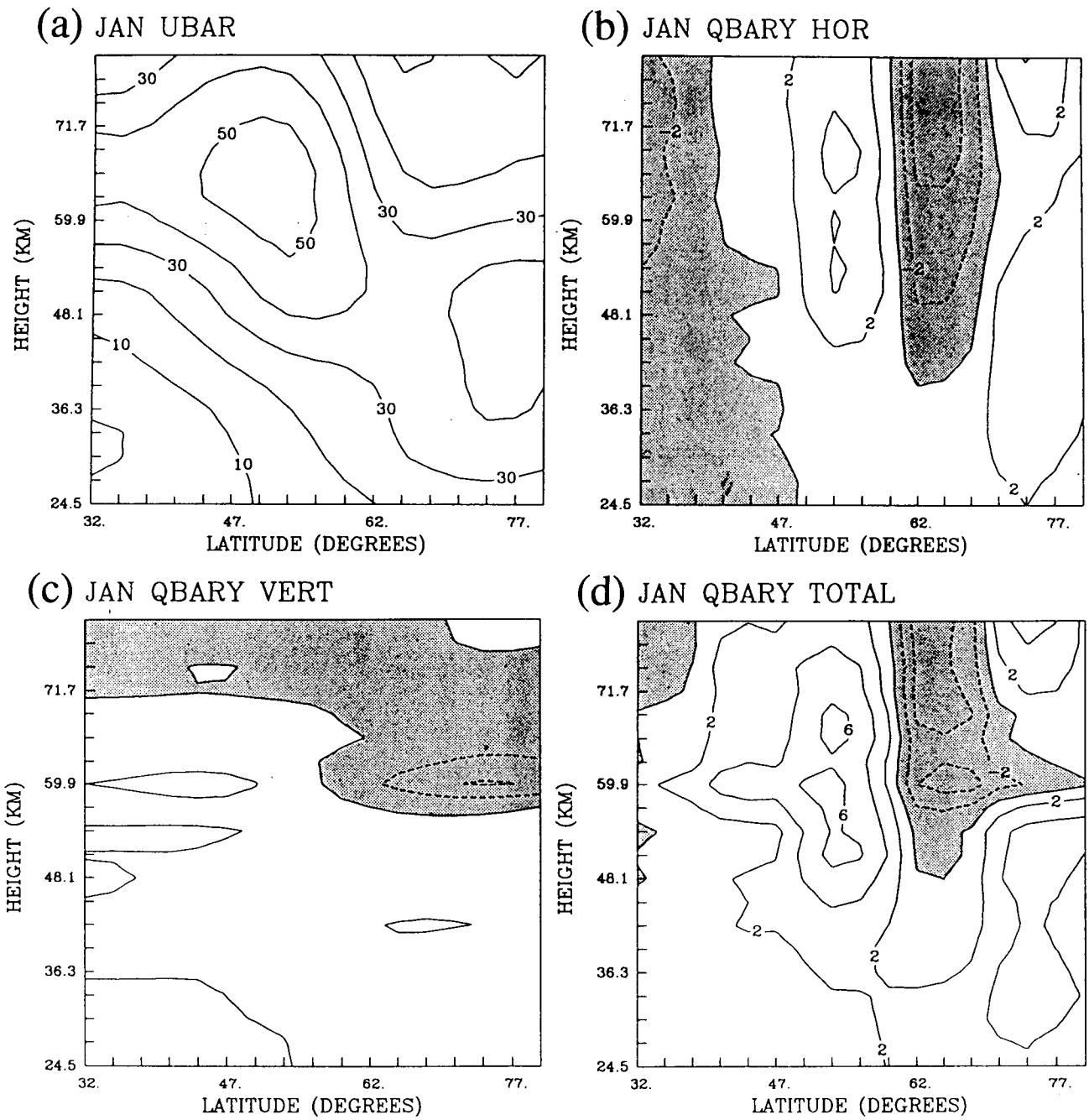

FIG. 6. Climatological zonal-mean wind field and potential vorticity gradients for January in the Northern Hemisphere: (a) zonal-mean zonal wind in meters per second, (b) horizontal term, Q_H, in the potential vorticity gradient, (c) vertical term, Q_V, in the potential vorticity gradient, and (d) total PV gradient, $\bar{q}_y$.

The growth rates for unstable modes are faster in the Southern Hemisphere than in the Northern Hemisphere. This is consistent with the observation that the 4-day wave is stronger in the Southern Hemisphere (Venne and Stanford 1982). The runs here are all made with climatological data; it is expected that potential vorticity gradients in synoptic data could be considerably stronger for short periods of time, which would result in stronger instability, or possibly an instability that is predominantly either baroclinic or barotropic in character. This is especially true in the Northern Hemisphere where the flow is more variable, and thus less closely resembles the time- and zonal-mean states used here. The appearance of relatively short *e*-folding

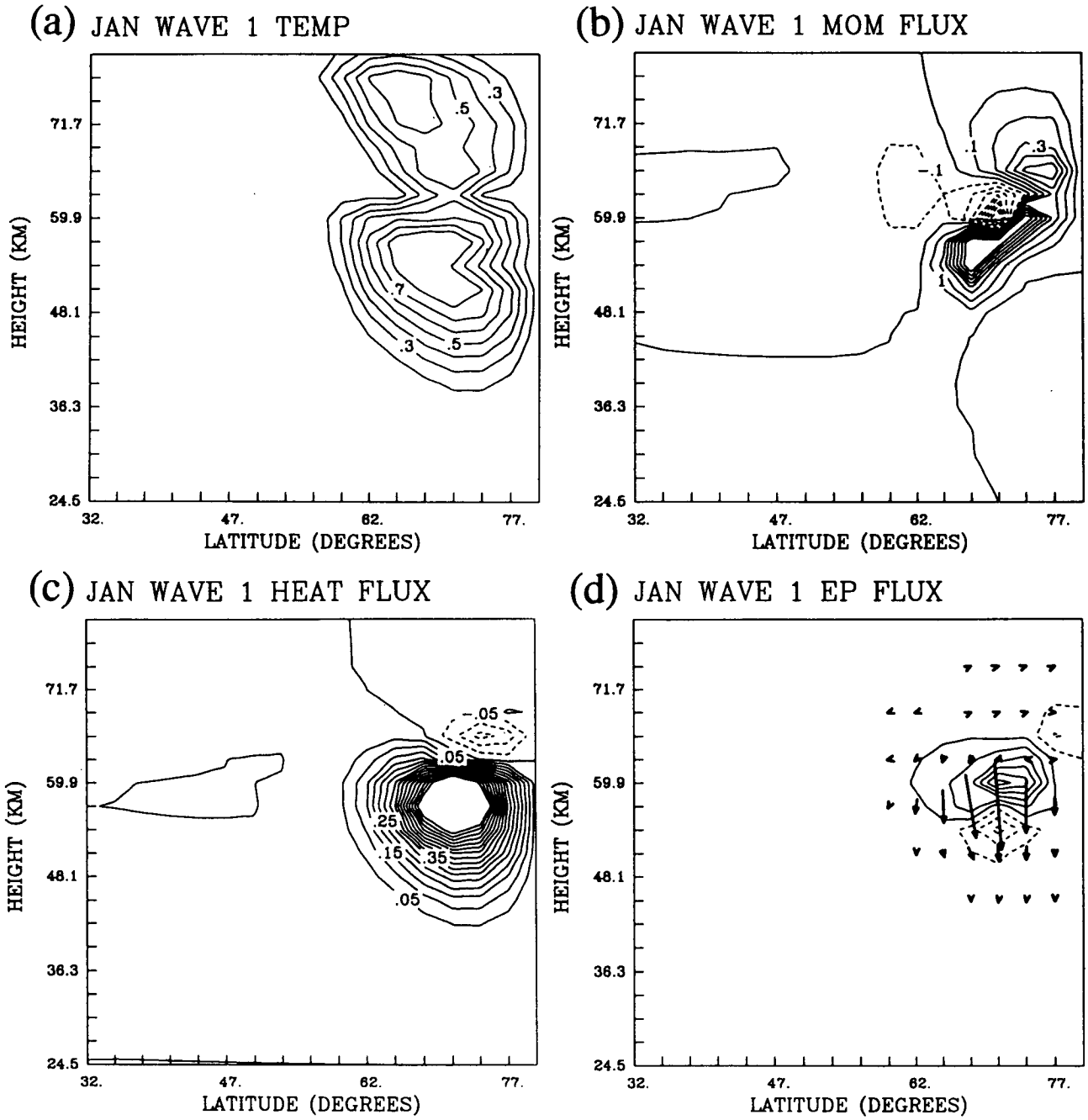

FIG. 7. Results from stability model for January basic state. (a) Perturbation temperature field for most unstable wave 1 mode, with maximum value normalized to 1; (b) perturbation momentum fluxes and (c) perturbation heat fluxes, scaled so that the relative amplitudes are as they would be if using MKS units; and (d) Eliassen–Palm (EP) flux and EP flux divergence for wave 1 unstable mode. Positive values (solid lines) show equatorward heat and momentum fluxes in (b) and (c).

times, some less than 5 d, for climatological basic states strongly suggests that this type of mode could be sufficiently unstable to be observed in the real atmosphere.

The characteristics of the unstable modes described above are consistent with one observed episode of 4-day wave growth, and with the known (i.e., equatorward momentum flux, largest amplitudes near the stratopause) characteristics of many others. The results of this study, and of previous stability studies focused on stability of the stratospheric polar night jet, suggest that there are, during most of the winter, large regions in the upper stratosphere and mesosphere where nec-

essary and sufficient conditions for instability are fulfilled. The exact nature of instabilities that occur, and hence, the characteristics of the 4-day wave, depend on the particular region that is most unstable at a given time. The periods are all near 4 days due to similar wind speeds in the background flow upon which these modes grow.

Acknowledgments. We thank Dr. Lee S. Elson for the use of the stability model. The research at JPL described in this paper was carried out by the Jet Propulsion Laboratory/California Institute of Technology, under a contract with the National Aeronautics and Space Administration. W. J. Randel was supported by NASA Grant W-16215.

REFERENCES

Elson, L. S., 1989: Three-dimensional linear instability modeling of the cloud level Venus atmosphere. *J. Atmos. Sci.*, **46,** 3560–3568.

——, 1990: Satellite observations of instability in the middle atmosphere. *J. Atmos. Sci.*, **47,** 1065–1074.

Fleming, E. L., S. Chandra, M. R. Schoeberl, and J. J. Barnett, 1988: Monthly mean global climatology of temperature, wind, geopotential height, and pressure for 0–120 km. NASA Tech. Memo. 100697, 85 pp.

Hartmann, D. L., 1983: Barotropic instability of the polar night jet stream. *J. Atmos. Sci.*, **40,** 817–835.

Lait, L. R., and J. L. Stanford, 1988: Fast, long-lived features in the polar stratosphere. *J. Atmos. Sci.*, **45,** 3800–3809.

Manney, G. L., 1991: The stratospheric 4-day wave in NMC data. *J. Atmos. Sci.*, **48,** 1798–1811.

——, T. R. Nathan, and J. L. Stanford, 1988: Barotropic stability of realistic stratospheric jets. *J. Atmos. Sci.*, **45,** 2545–2555.

Plumb, R. A., 1983: A new look at the energy cycle. *J. Atmos. Sci.*, **40,** 1669–1688.

Prata, A. J., 1984: The 4-day wave. *J. Atmos. Sci.*, **41,** 150–155.

Randel, W. J., and L. R. Lait, 1991: Dynamics of the 4-day wave in the Southern Hemisphere polar stratosphere. *J. Atmos. Sci.*, **48,** 2496–2508.

Simmons, A. J., 1974: Baroclinic instability at the winter stratopause. *Quart. J. Roy. Meteor. Soc.*, **100,** 531–540.

Venne, D. E., and J. L. Stanford, 1979: Observations of a 4-day temperature wave in the polar winter stratosphere. *J. Atmos. Sci.*, **36,** 2016–2019.

——, and ——, 1982: An observational study of high-latitude stratospheric planetary waves in winter. *J. Atmos. Sci.*, **39,** 1026–1034.